Organic Optics and Electronics

Academic and Research Staff
Prof. V. Bulović, Dr. Corinne Packard, Dr. Matthew Panzer, Dr. Jonathan (Yaakov) Tischler, Dr. Burag Yaglioglu, Dr. Ni Zhao

Visiting Scientists and Research Affiliates
T. Bloomstein (Lincoln Laboratory), T. Etheridge (HP), F. Jaworski (Raytheon), L. Rolly (HP)

Graduate Students
G. Akselrod, P. Anikeeva, A. Arango, S. Bradley, D. Friend, J. Ho, Q. Hu, T. Osedach, S. Paydavosi, J. Rowehl, Y. Shirasaki, H. Tang, V. Wood, J. Yu

Technical and Support Staff
M. Pegis, Admin. Asst.

1. Electroluminescence from Phosphor-doped Nanocrystals

Sponsors
Institute for Soldier Nanotechnologies, PECASE, NDSEG

Project Staff
V. Wood, J. E. Halpert, M. J. Panzer, M.G. Bawendi, V. Bulović

Alternating current thin-film electroluminescent (AC-TFEL) devices already occupy a segment of the large-area, high-resolution, flat-panel-display market. The AC-TFEL displays, which consist of a phosphor layer, such as manganese doped-zinc sulfide (ZnS:Mn), vertically sandwiched between two insulators that are contacted by electrodes, are robust, possess long lifetimes, and offer high luminance with relatively low power consumption [1], [2]. While fabrication of AC-TFEL devices has been the subject of considerable study over the past three decades, significant challenges remain. Development of multicolor displays with balanced red, green, and blue (RGB) emission has proven difficult as the most efficient red, green, and blue phosphors comprise different materials systems that require different deposition and annealing steps. Transparent AC-TFEL displays have recently been demonstrated by Sharp, Inc.; however, the processing of the phosphor to achieve transparency is difficult and has not yet been developed for phosphors other than ZnS:Mn [3].

We present a novel materials system for solution processing of the active phosphor layer in transparent AC-TFEL devices. We use colloidally-synthesized Mn-doped nanocrystals interspersed between RF magnetron sputtered ZnS layers to demonstrate electroluminescence (EL) from a solution-deposited active layer in an AC-TFEL device fabricated at room temperature [4]. We adapt the synthesis of Thakar *et al*. to make stable ZnSe/ZnS:Mn/ZnS nanocrystals with quantum yields of (65±5)% [5]. As Figure 1 shows, these wide band gap host nanocrystals along with sputtered wide band-gap metal oxides (Al_2O_3, HfO_2, and ITO) enable transparent AC TFEL devices without additional processing steps beyond the room-temperature layer-by-layer deposition of each material set. Our devices exhibit electroluminescence from the Mn dopants at frequencies greater than 10 kHz and with voltages as low as 110 V_{pp} (See Figures 1 and 2) [4].

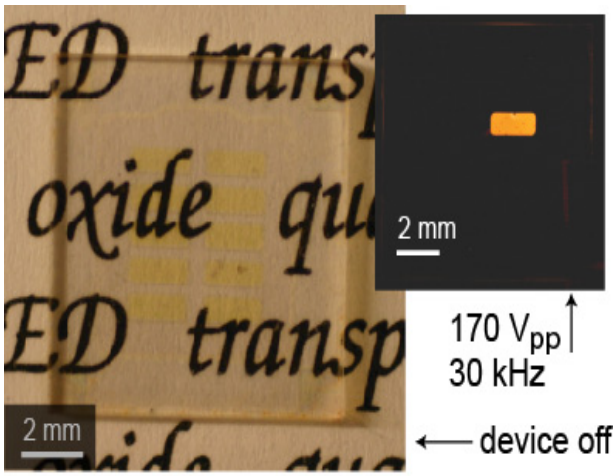

Figure 1: A photograph of a 0.5 in. x 0.5 in. glass substrate containing ten 1 mm x 2 mm AC-TFEL devices, with no bias applied. The substrate is pictured on top of printed text to demonstrate the transparency of our AC-TFEL device architecture. The inset shows the uniformity of pixel illumination (in the dark) with the device operating at 170 V_{pp} and 30 kHz.

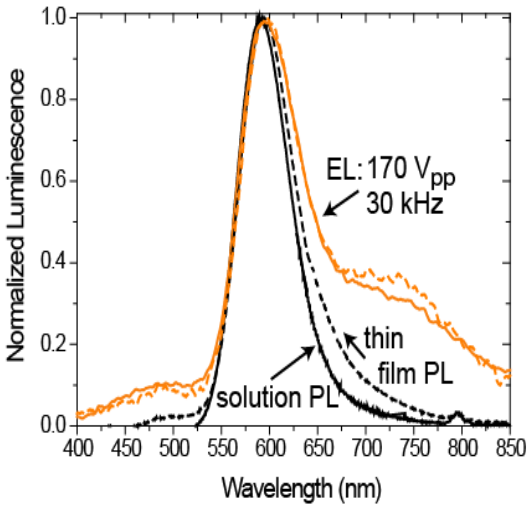

Figure 2: Electroluminescent (EL) spectra for devices with Al_2O_3 and HfO_2 insulating layers (solid and dashed orange curves, respectively). Photoluminescence (PL) spectra of the nanocrystal solution (solid gray curve) and a completed device (dashed black line). The overlap of the spectral peaks indicates that the emission is due to the Mn impurity dopants.

References

Y. A. Ono, Electroluminescent Displays. Singapore: World Scientific, 1995.

J.P. Keir and J.F. Wager, "Electrical Characterization of Thin-Film Electroluminescent Devices," Annu. Rev. Mat. Sci., vol 27, 1997, pp. 223-248.

A. Abileah, K. Harkonen, A. Pakkala, and G. Smid. Transparent Electroluminescent (EL) Diplays, Planar Systems, 2008.

V. Wood, J.E. Halpert, M.J. Panzer, M.G. Bawnedi, and V. Bulović. "AC-driven Electroluminescence from ZnSe/ZnS:Mn/ZnS Nanocrystals," Nano Lett. in press, 2009.

R. Thakar, Y. Chen, and P.T. Snee, "Efficient Emission from Core/(Doped) Shell Nanoparticles: Applications for Chemical Sensing," Nano Lett., vol. 7, no. 11, Oct. 2007., pp. 3429-3432.

2. Low-threshold Coherently-coupled Organic VCSEL

Sponsors

Institute for Soldier Nanotechnology

Project Staff

J. R. Tischler, E. R. Young, D. G. Nocera, V. Bulović

Here we report observation of extremely low-threshold lasing in organic VCSELs when the excitons are coherently coupled non-radiatively to each other. Non-radiative coupling between excitons can enhance the emission cross-section of a gain material and lead to laser action at considerably lower excitation densities [1]. The coupling strength associated with the excitonic interaction is proportional to the number of excited molecules at any given time; hence the effect necessitates creating the exciton population quickly relative to the excited state decay time. This phenomenon is often referred to as superradiance [1], [2]. In organic semiconductor VCSELs, this effect leads to a 95% reduction in threshold when sub-psec non-resonant excitation is utilized to create the exciton population, instead of a longer nsec duration pump pulse. The VCSELs consist of a thermally evaporated gain layer composed of the laser dye DCM doped (2.5 % v/v) into an Alq_3 host matrix, which is situated between a metal mirror and a dielectric Bragg

reflector (DBR). In VCSELs where the gain layer is "λ/2n thick", i.e., 156.7 nm, an extremely low threshold of 4.9 μJ/cm^2 is observed. This marks the first time lasing from organics has been reported in a metal/DBR half-wavelength thick microcavity, despite the rather modest resonator quality factor of Q < 200. Lasing is confirmed by supra-linear input-output power dependence and by spectral and spatial line-narrowing above the threshold. Moreover, when the optical excitation is polarized, the emission above the threshold strongly follows the polarization of the pump light. All prior demonstrations of laser action in solid-state organic VCSEL structures have utilized either gain layers of at least 3 times the thickness [3] or have relied on higher finesse of all dielectric microcavities [4]. The observed laser threshold of 4.9 μJ/cm^2 in the half-wavelength thick microcavity corresponds to excitation of at most 3.2% of the DCM molecules.

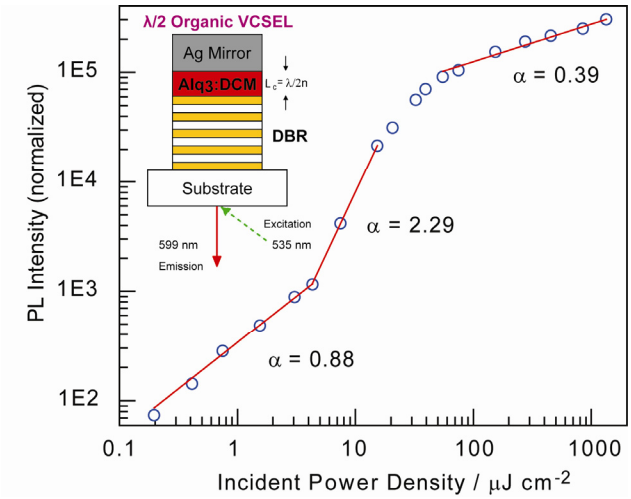

Figure 1: Input/Output power dependence upon direct DCM excitation (λ_{ex} = 535 nm) shows the lasing threshold at 4.9 μJ/cm^2 incident power and superlinear slope α = 2.29 when fit to power law, y = mx$^{\alpha}$. Inset: Device design consists of a dielectric Bragg reflector (DBR), organic semiconductor gain layer, and silver mirror. The sample is excited at θ = 60° from normal using TM polarized laser light focused down to a spot size of 0.001 cm^2 as measured on the sample plane.

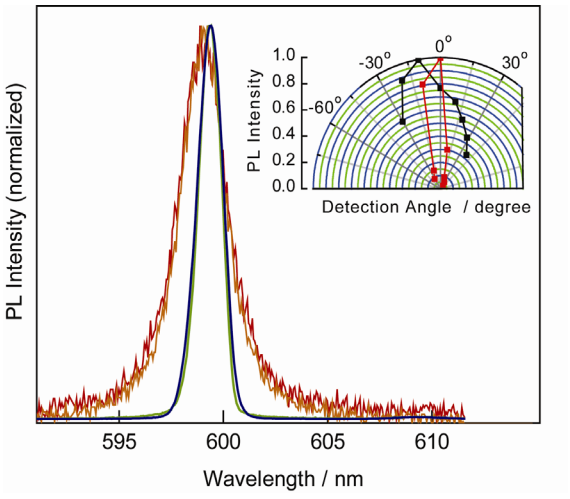

Figure 2: Emission spectra of OVCSEL at different power levels above and below the threshold show linewidth narrowing from 2.5 nm for excitation below threshold (▬, 3.25 μJ/cm^2; ▬, 8 μJ/cm2) to 1.1 nm above threshold (▬, 15 μJ/cm^2; ▬, 250 μJ/cm^2). Inset: Emission cone spatially narrows from from Δθ = ± 30° to Δθ = ± 5° as measured at the emission peak.

References

L. Moi, P. Goy, M. Gross, J. M. Raimond, C. Fabre, and S. Haroche, "Rydberg-atom masers. I. A theoretical and experimental study of super-radiant systems in the millimeter-wave domain", Physical Review A, vol. 27, pp. 2043-2064, April 1983.

R. H. Dicke, "Coherence in Spontaneous Radiation Processes", Physical Review, vol. 93, pp. 99-110, January 1954.

V. Bulović, V. G. Kozlov, V. B. Khalfin, and S. R. Forrest, "Transform-limited, narrow-linewidth lasing action in organic semiconductor microcavities", Science, vol. 279, pp. 553-555, January 1998.

M. Koschorreck, R. Gehlhaar, V. G. Lyssenko, M. Swoboda, M. Hoffmann, and K. Leo, "Dynamics of a high-Q vertical-cavity organic laser", Applied Physics Letters, vol. 87, pp. 181108:1-3, October 2005.

3. Heterojunction Photovoltaics Using Printed Colloidal Quantum Dots

Sponsors
Institute for Soldier Nanotechnologies, DOE Solar America Program

Project Staff
A.C. Arango, S. Geyer, M.G. Bawendi, V. Bulović

Colloidal quantum dot (QD) systems offer distinct optical and electronic properties that are not easily attained by other nanostructured semiconductors, such as highly saturated emission in QD light-emitting-diodes, access to infrared radiation in QD photodetectors, and the prospect of optically optimized solar cell structures [1]. The prevailing deposition method for colloidal QD systems is spin-casting, which introduces limitations such as solvent incompatibility with underlying films and the inability to pattern side-by-side pixels for multispectral photodetector arrays. In the present work we employ a non-destructive microcontact printing method [2], which allows for deposition of a thin quantum dot film onto a wide-band-gap organic hole transport layer, N,N'-Bis (3-methylphenyl)-N,N'-bis-(phenyl)-9,9-spiro-bifluorene (spiro-TPD), thus producing an inorganic/organic heterojunction that serves to enhance charge separation in the device. The top and bottom contacts are provided by ITO electrodes, allowing for near-transparency (Figure 1).

Restrictions imposed by transport losses in the QD film are found to limit charge generation. Measurements of the external quantum efficiency (EQE) and internal quantum efficiency (IQE) as a function of QD film thickness, plotted in Figure 2, reveal a marked dependence on thickness. The IQE is determined by dividing the EQE by the absorption of the QD film, all of which are measured at the first absorption peak of the QD film (λ = 590 nm). Following excitation and exciton diffusion to an interface, dissociation of the exciton produces free carriers that must diffuse to opposite electrodes in order to produce a photocurrent. A model that accounts for both exciton and charge diffusion reproduces the general thickness trend, assuming an exciton diffusion length L_{Ex} = 43 nm, an electron diffusion length L_{El} = 61 nm, and near-zero contribution from the first two QD monolayers. Further development will require reducing exciton and charge transport losses in order to permit efficient charge-generation from thicker QD films with improved absorption.

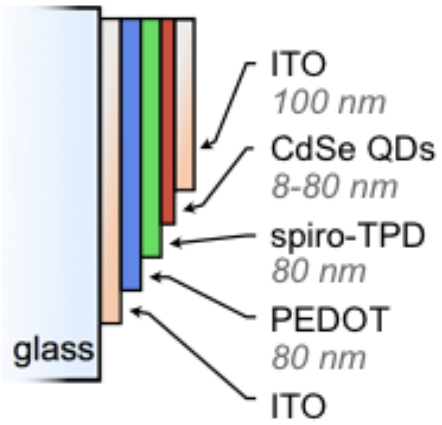

Figure 1: The QD heterojunction device architecture used in this work accommodates QD film thicknesses varying from 8 to 80 nm.

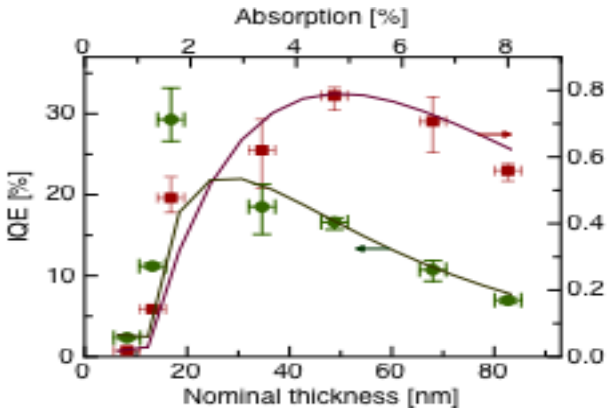

Figure 2: External quantum efficiency (EQE) (red squares) and internal quantum efficiency (IQE) (green circles) at λ = 590 nm versus nominal QD film thickness and device absorption at λ = 590 nm. An analytical model for the EQE (red line) and IQE (green line) reproduces the general trend with thickness. Nominal thicknesses are calculated assuming an absorption coefficient of 10^4 cm^{-1} at λ = 590 nm.

References

D.C. Oertel, M.G. Bawendi, A.C. Arango, and V. Bulović. "Photodetectors based on treated CdSe quantum-dot films," Applied Physics Letters, vol. 87, no. 21, p. 213505, Nov. 2005.

A. C. Arango, D. C. Oertel, Y. Xu, M. G. Bawendi, and V. Bulović. "Heterojunction photovoltaics using printed colloidal quantum dots as a photosensitive layer," Nano Letters, vol. 9, no. 2, pp. 860–863, Feb. 2009.

4. Heterojunction Photodetector Consisting of Metal-oxide and Colloidal Quantum-dot Thin Films

Sponsors
Institute for Soldier Nanotechnologies, DOE Solar America Program

Project Staff
T. P. Osedach, N. Zhao, L.-Y. Chang, S. M. Geyer, A. C. Arango, J. C. Ho, M. Bawendi, V. Bulović

We demonstrate a heterojunction photodetector consisting of a metal-oxide charge transport layer and a colloidal quantum-dot (QD) charge-generation layer. To make the device, a metal-oxide semiconductor, SnO_2, is sputter-deposited over an array of interdigitated gold electrodes. A thin film of PbS QDs is then spin-coated over the structure (see Figure 1a). The optical and electrical characteristics of the device can be optimized independently through the modification of these two layers.

The metal-oxide and QD layers form a type-II hetero-interface (Figure 1b) suitable for dissociating photo-generated excitons. Exciton dissociation at the interface results in the generation of holes in the QD layer and electrons in the metal-oxide layer. A bias corresponding to a field of ~10^4 V/cm is applied across the electrodes to facilitate carrier collection. The increased electron density increases the metal-oxide film conductivity, which in turn manifests an increase in lateral current through the device. A plot of the spectrally resolved external quantum efficiency is shown in Figure 2, with high efficiency response matching the spectral response of quantum-dot absorption.

This work builds on previous reports from our laboratory in which an organic/organic photodetector [1] and an organic/QD photodetector [2] were described. The present device can be driven at reduced bias and extends spectral sensitivity into the infrared region. The unique ability to independently tune the optical and electrical characteristics of these structures makes them a valuable platform with which to study the physical processes at QD hetero-interfaces.

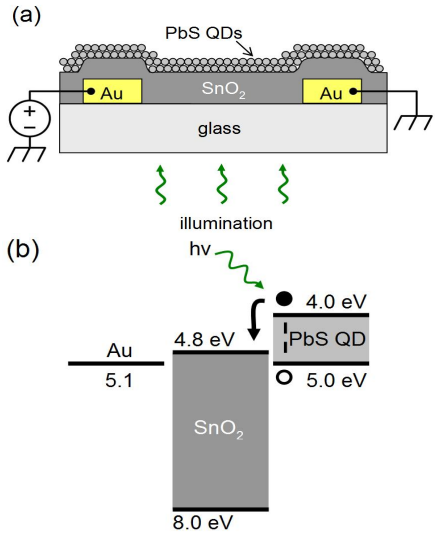

Figure 1: (a) Schematic of the device structure. (b) Energy band diagram. Excitons dissociate at the interface between the metal-oxide film and the quantum dots.

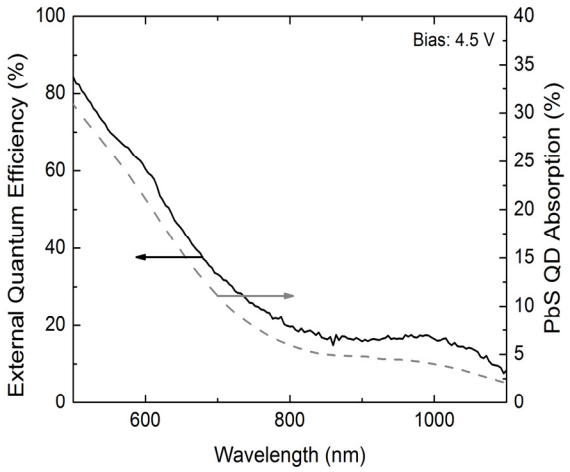

Figure 2: External quantum efficiency spectrum (solid) and PbS QD absorption (dashed).

References:

J. Ho, A. Arango, and V. Bulović, "Lateral organic bilayer heterojunction photoconductors", Appl. Phys. Lett. 2008.

T. P. Osedach, S. M. Geyer, J. C. Ho, A. C. Arango, M. G. Bawendi, V. Bulović, "Lateral heterojunction photodetector consisting of molecular organic and colloidal quantum dot thin films", Applied Physics Letters, January 2009.

5. Heterojunction Photoconductors for Chemical Detection

Sponsors
Institute for Soldiers Nanotechnology, Center for Materials Science and Engineering

Project Staff
J. C. Ho, J. A. Rowehl, V. Bulović

We have developed and demonstrated a solid-state sensor platform that directly transduces the chemosignal of a fluorescent polymer-chemical interaction into photocurrent. In addition to the direct transduction mechanism, the sensor separates the chemosensing and conduction processes across the two different films, enabling independent optimization of each film to serve a specific function [1]. Conceptually, the device consists of a Type-II bilayer heterojunction deposited on planar electrodes that enables the application of an electric field in-plane with the interface. The bilayer heterojunction is realized by spin-casting a chemosensitive fluorescent polymer on top of a sputtered metal oxide film.

Figure 1 depicts device operation: 1) absorption of illumination creates excitons, 2) excitons diffuse to the interface, 3) band offsets enable efficient exciton dissociation into free carriers, and 4) transport of photogenerated, free carriers in the photoconductive channel. The presence of an analyte will strongly modulate the photoluminescence (PL) efficiency of the chemosensitive fluorescent polymer, which signifies a change in the population of excitons that can radiatively decay [2] . Altering the exciton population changes the carrier concentration at the heterointerface, which results in a change in the measured photocurrent.

Initial testing of bilayer sensors, incorporating various polymers as the EGL and SnO_2 (doped 30% O_2) as the CTL, demonstrates an upper sensitivity limit to TNT detection of approximately 10 picograms of material in a few seconds. Figure 2 compares the spectral response of a 100-nm film of SnO_2 to a bilayer device (100 nm SnO_2/5nm HW polymer) before and after exposure to saturated TNT vapor. The inset shows the real-time change in photoconductivity at the absorption peak of the polymer when TNT vapor is introduced at time t = 0. These results prove the bilayer sensor concept and hold promise for the development of a sensitive, highly specific, portable chemical sensor platform with potential for a wide array of applications.

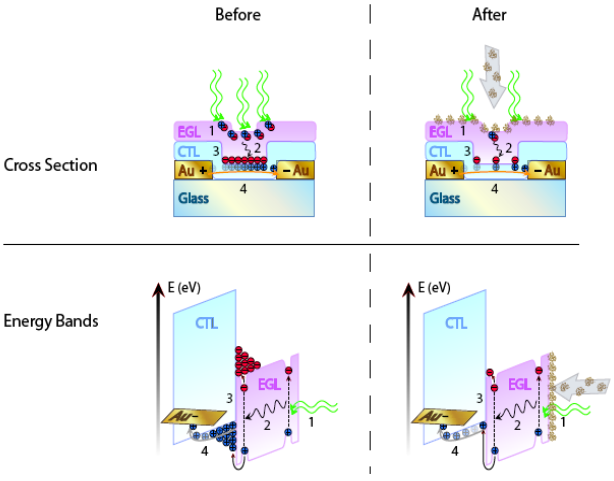

Figure 1: Energy band diagrams and cross-sections of bilayer sensor consisting of an exciton generation layer (EGL) and a charge transport layer (CTL) before and after exposure to a particular analyte.

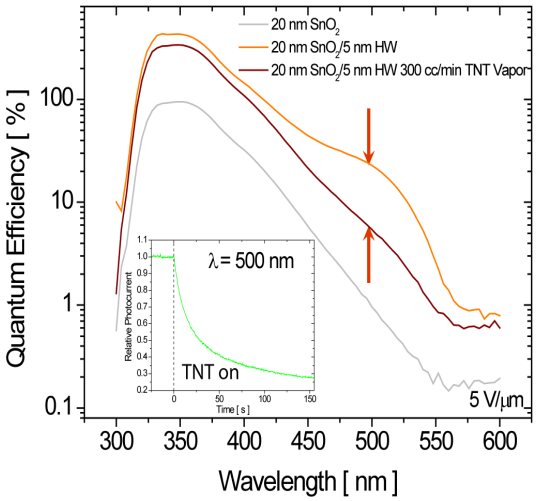

Figure 2: Semilogarithmic spectral response plot of HW polymer/SnO_2 bilayer sensor before (orange) and after (brown) saturated TNT vapor exposure. Response of 20-nm SnO_2 film (grey) is shown for comparison. Inset: Time response of TNT sensing action at t = 500 nm. TNT vapor is introduced at time t = 0 s.

References
J. Ho, A. Arango, and V. Bulović, "Lateral Organic Bi-layer Heterojunction Photoconductors," Applied Physics Letters, vol. 93, 063305, August 2008.
S. W. Thomas, G. D. Joly, and T. M. Swager, "Chemical Sensors Based on Amplifying Fluorescent Conjugated Polymers," Chemical Review, vol. 107, pp. 1339-1386, March 2007.

6. Multi-layer Heterojunction Photoconductors

Sponsors
Institute for Soldiers Nanotechnology Center for Materials Science and Engineering

Project Staff
J. C. Ho, J. A. Rowehl, V. Bulović

We fabricate a two-terminal, lateral multi-layer photoconductor consisting of three molecular organic thin films with cascading energy bands (see Figure 1): the charge transport layer (CTL), N,N'-bis(3-methylphenyl)-N,N'-diphenyl-1,1'-biphenyl-4,4'-diamine (TPD); the charge spacer layer (CSL), N,N'-bis-(1-naphthyl)-N,N' –diphenyl-1,1-bipheny1-4,4'-diamine (NPD); and the exciton-generation layer (EGL), 3,4,9,10-perylenetetracarboxylic bis-benzimidazole (PTCBI). Placing an interstitial spacer layer between the CTL and the EGL improves the photogenerated current of tri-layer photoconductors over bi-layer, Type-II heterojunction photoconductors.

Light excitation acts as a pseudo- "gate electrode" by generating excitons in PTCBI (EGL). Those excitons diffuse to the PTCBI/NPD interface, where they dissociate, leaving the electron behind in PTCBI, while the hole is initially injected into NPD from where it can transfer to the more energetically favorable states in TPD. Excess holes in the TPD film raise the hole-carrier concentration in the TPD film and increase the device conductance by forming a channel of excess carriers at the TPD/NPD interface. The thin film of NPD (CSL), between TPD (CTL) and PTCBI (EGL), spatially separates the dissociated carriers, reducing the likelihood of bimolecular recombination across the TPD/PTCBI interface. Bi-layer heterojunction photoconductors consisting of TPD and PTCBI alone have been shown to improve the external quantum efficiency over single layers of TPD and PTCBI by several orders of magnitude [1], [2]. Measurement of the current at an optical excitation wavelength of 532 nm from a biased multi-layer, lateral heterojunction device [Au/TPD(50 ± 0.5) nm/NPD(4 ± 1) nm/PTCBI(50 ± 0.5) nm] displays improvement by a factor of eight over the bi-layer without a CSL (see Figure 2). A thickness study of the NPD spacer layer experimentally demonstrates the dependence of the photoresponse efficiency on the spatial separation of the dissociated charge.

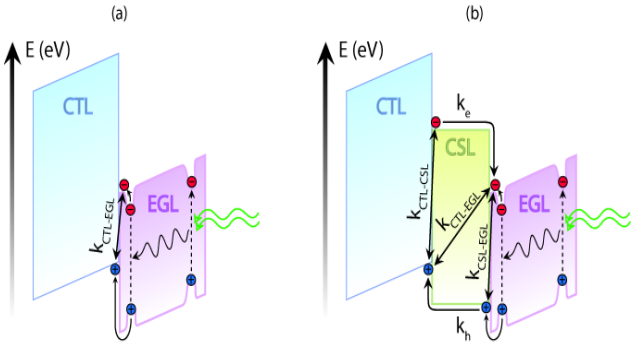

Figure 1: Energy-band diagrams of (a) a bilayer device consisting of CTL/EGL and (b) a trilayer device consisting of CTL/CSL/EGL. Relevant interfacial recombination rates and carrier diffusion rates are depicted.

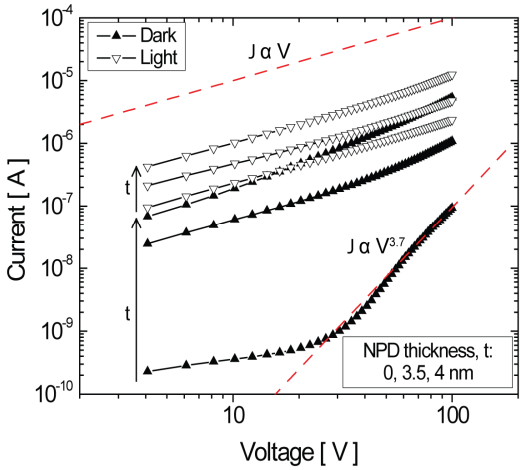

Figure 2: Log-log current-voltage characteristics of TPD 50 ± 0.5 nm TPD/NPD/50 ± 0.5 nm PTCBI, with 0, 3.5, and 4 nm of NPD. Arrows indicate increasing NPD thickness and dashed red lines are guides that depict ohmic and trap-limited conduction.

References

J. Ho, J. Rowehl, and V. Bulović, "Organic Multi-layer Lateral Heterojunction Phototransistors," presented at Electronic Materials Conference, Santa Barbara, CA, June 2008.

J. Ho, A. Arango, and V. Bulović, "Lateral Organic Bi-layer Heterojunction Photoconductors," Applied Physics Letters, vol. 93, 063305, August 2008.

7. Three-molecular-layers-thick J-aggregate Photoconductor

Sponsors

MIT Institute for Soldier Nanotechnologies, Solar Revolutions Center at MIT, NSF Materials Research Science and Engineering Center at MIT

Project Staff

Y. Shirasaki, J. Ho, M. S. Bradley, J. R. Tischler, V. Bulović

Due to their record high absorption constant and narrow photoluminescence linewidth [1], thin films of J-aggregated cyanine dyes have been extensively studied with respect to their potential applications in novel opto-electronic devices, such as organic light emitting diodes, optical switches, and lasers. J aggregates' strong absorption is especially interesting for use in light sensing devices like a photoconductor. A J-aggregate film that is only a few nanometers thick, in conjunction with a dielectric mirror, has an ability to absorb almost 100% of incoming light [2] at normal incidence.

We demonstrate in this study an efficient lateral J-aggregate photoconductor. Our device structure is a bi-layer heterojunction consisting of an optically active 5 nm thick TDBC J-aggregate thin film, which serves as the primary exciton generation layer, and a 50 nm layer of zinc indium oxide (ZIO) underneath, which serves as a charge transport layer. The contacts which sit below the ZIO are series of gold interdigitated fingers photolithographically defined on glass. The bi-layer structure physically separates the light absorption and charge transport regions of the device, taking advantage of the J aggregates' unique optical properties and the ZIO's charge transport properties. We observe that the heterojunction significantly increases the efficiency of the device by assisting the dissociation of the excitons, similar to the work reported by J. Ho *et al* [3]. External quantum efficiency (EQE), defined as the change in number of electrons passing through the bi-layer device per incident photon is shown in Figure 1. EQE greater than 100 % suggests that the exciton recombination lifetime is greater than the transit time of the electrons passing through the device. The curve follows the absorption curve of ZIO and the J aggregates shown in the inset. Figure 2 shows the time response of the bi-layer device.

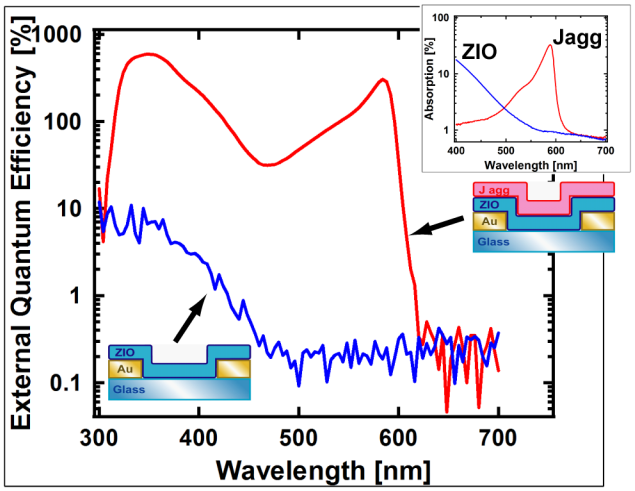

Figure 1: External quantum efficiency of the bi-layer device as a function of the incident light wavelength. The inset is the absorption curves of ZIO and TDBC J aggregates. The efficiency of the device is significantly improved where the J aggregates absorb light.

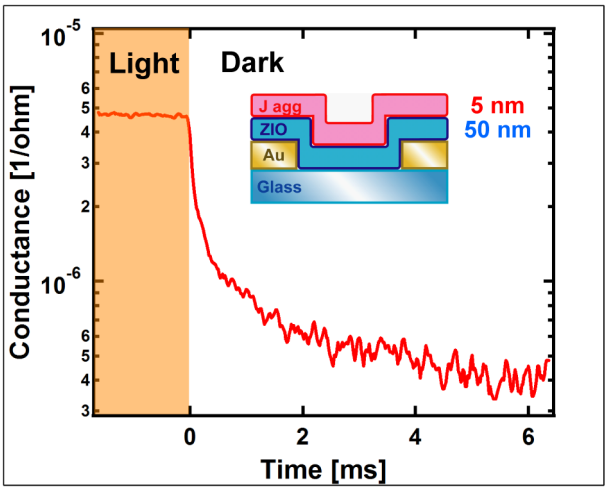

Figure 2: Time response of the bi-layer device using a LED light source peaked around 595 nm.

References:

M. S. Bradley, J. R. Tischler and V. Bulović, "Layer-by-layer J-aggregate thin films with a peak absorption constant of 10^6 cm^{-1}," Advanced Materials, vol. 17, no. 15, pp. 1881-1886, August 2005.

J. R. Tischler, M. S. Bradley and V. Bulović, "Critically coupled resonators in vertical geometry using a planar mirror and a 5 nm thick absorbing film," Optics Letters, vol. 31, no. 13, pp. 2045-2047, July 2006.

J. C. Ho, A. Arango and V. Bulović, "Lateral organic bilayer heterojunction photoconductors," Applied Physics Letters, vol. 93, no. 6, pp. 063305, August 2008.

8. Patterned Organic Microcavities for Confinement of Exciton-Polaritons

Sponsors
NDSEG, Institute for Soldier Nanotechnologies

Project Staff
M. S. Bradley, J. R. Tischler, G. Akselrod, V. Bulović

We demonstrate fabrication of organic laterally-patterned microcavity devices with lateral sizes on the micron scale using PDMS lift-off patterning. Recently, low-threshold lasing was demonstrated from pillars formed by thermally evaporating thin films of Alq_3 (aluminum tris(8-hydroxyquinoline)) doped with the laser dye DCM (4-(dicyanomethylene)-2-methyl-6-(4-dimethylaminostyryl)-4H-pyran) through thin nickel shadow masks with square, 5- x 5-nm^2 openings [1]. Additionally, recent research efforts in microcavity exciton-polariton devices based on inorganic active materials such as GaAs or CdTe quantum wells have focused on the lateral patterning of microcavity exciton-polariton systems [2]. Such 0D cavities allow for symmetry-breaking of the in-plane wave vector, opening new pathways for parametric generation of photon pairs [3]. For the same reason, laterally-patterned organic microcavity exciton-polariton devices are also of interest. The PDMS lift-off patterning, as opposed to shadow masking, allows standard lithography techniques to be used to define pattern features in silicon PDMS molds [4], [5]. Additionally, smaller features than are achievable through shadow masking are theoretically feasible even with PDMS due to the generally low aspect ratio in PDMS needed for embossing small features on the patterned organic film.

We use PDMS lift-off patterning of a thin film of thermally-evaporated TPD (N′-bis(3-methylphenyl)-N,N′-diphenyl-1,1′-biphenyl-4,4′-diamine) doped with DCM to form embossed pillars in the TPD film of 20-25 nm in thickness. Figure 1a shows the device structure, Figure 1b shows PDMS lift-off patterning technique, and Figure 1c shows the molecular diagrams of the device constituents. When the sample is optically excited with a [=408 nm light source, emission from both the unpatterned ([~630 nm) and patterned areas ([~655 nm) is observed, as seen in Figure 2. The background emission dominates since its cavity resonance is closer to the resonance of DCM, as shown; use of different organic materials with larger lift-off amounts can increase this wavelength shift.

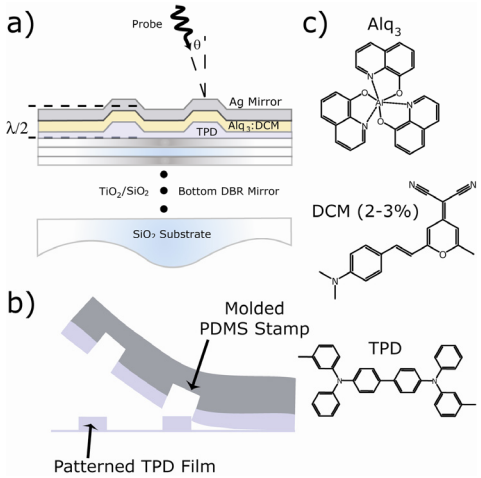

Figure 1: (a) Patterned microcavity structure. (b) The PDMS lift-off patterning process. (c) Molecular structures of constituent materials.

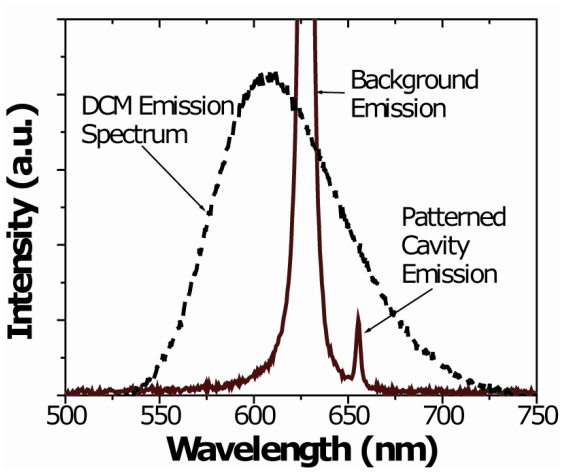

Figure 2: Emission spectrum of DCM with unpatterned (background) and patterned microcavities when excited with λ=408 nm.

References

M. Sudzius, M. Langner, S. I. Hintschich, V. G. Lyssenko, H. Frob, and K. Leo, "Multimode laser emission from laterally confined organic microcavities," Applied Physics Letters, vol. 94, 2009.

O. El Daif, A. Baas, T. Guillet, J. P. Brantut, R. I. Kaitouni, J. L. Staehli, F. Morier-Genoud, and B. Deveaud, "Polariton quantum boxes in semiconductor microcavities," Applied Physics Letters, vol. 88, 2006.

D. Bajoni, E. Peter, P. Senellart, J. L. Smirr, I. Sagnes, A. Lemaitre, and J. Bloch, "Polariton parametric luminescence in a single micropillar," Applied Physics Letters, vol. 90, 2007.

J. Yu and V. Bulović, "Micropatterning metal electrode of organic light emitting devices using rapid polydimethylsiloxane lift-off," Applied Physics Letters, vol. 91, 2007.

J. Yu, “Improving OLED Technology for Displays,” Doctoral thesis, Elec. Eng. and Comp. Sci., Mass. Inst. of Tech., Cambridge, MA, 2008.

9. Exciton-Exciton Annihilation in Organic Polariton Microcavities

Sponsors
CMSE, RLE, Hertz Foundation

Project Staff
G. M. Akselrod, J. R. Tischler, E. R. Young, M. S. Bradley, D. G. Nocera, V. Bulović

Excitons in a solid can be coupled to the electromagnetic field by placing the material inside a resonantly tuned microcavity. If the decay rates of the excitons and the cavity mode are slower than the rate of energy exchange, the system takes on new eigenstates that are light-matter superpositions known as exciton-polaritons, and the limit of strong coupling is achieved. Recent work has demonstrated the use of organic thin films [1], [2] as the excitonic layer in polaritonic structures and the characteristic linear properties of these devices showed strong coupling. We present the first in-depth study of high-intensity optical excitation of such organic exciton-polariton devices.

The excitonic component of our devices was made of the 5.1 ± 0.1 nm film of J-aggregated cyanine dye TDBC assembled using layer-by-layer growth [3], giving an extremely high absorption coefficient of 10^6 cm^{-1}. The cavity was formed by sputter-depositing a 4.5 pair distributed Bragg reflector (DBR) on a quartz substrate, followed by a λ/4n SiO_2 spacer layer, where n is the index of refraction and λ = 595 nm, the peak of the J-aggregate emission (Figure 1a). The J-aggregate film was then deposited, followed by a 100±1 nm spin coated layer of polyvinyl alcohol, which enhances the photoluminscence quantum yield of the J-aggregate film and acts as a spacer layer. A transparent thermally evaporated organic layer forms the remainder of the spacer, and the structure is capped with silver mirror, giving a cavity Q of ~60. The reflectivity as well as the photoluminscence (PL) of these devices shows two distinct resonances, which is characteristic of strong coupling (Figure 1).

To test for evidence of polariton lasing, the devices were pumped at λ = 535 nm at 60° relative to normal and the PL was collected at normal incidence. To fully characterize the behavior of the devices in a wide range of power regimes, three pump sources were utilized: a CW laser at 532 nm, a 10-ns pulsed laser at 535 nm, and a 150-fs pulsed laser at 535 nm. With CW excitation, all of the devices showed linear PL intensity as a function of input power. With 10-ns excitation, the PL began to show a sublinear power law dependence (p = 0.535), with the effect becoming more pronounced with 150-fs excitation (p = 0.348) (Figure 2a and b). Devices with a range of tunings as well as cavities with higher Q (~115) were tested and all showed the same qualitative sublinear behavior. A similar sublinear behavior was observed in J-aggregate thin films that were not situated in a cavity. We propose the process of exciton-exciton annhilation as a possible mechanism to explain the reduction of quantum yield with increasing intensity. Previous studies have shown the existence of exciton-exciton annihilation in cyanine dye J-aggregates [5], and it is a phenomenon observed in other excitonic materials that are candidates for organic polariton lasing. Annihilation would be a process directly in competition with polariton-polariton scattering—inherently an exciton-exciton interaction—which is a possible mechanism for populating the *k* = 0 state of the polariton dispersion and achieving room- temperature organic polariton lasing.

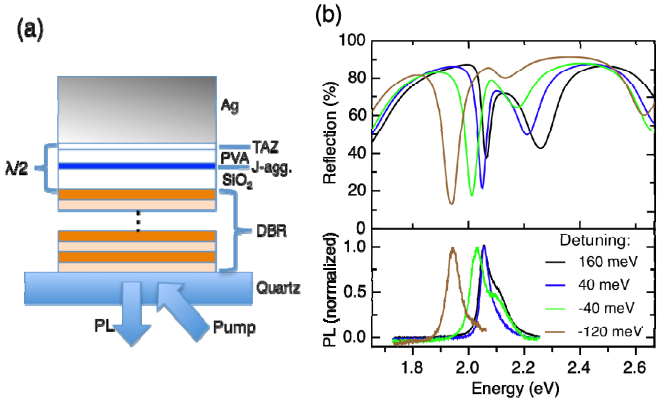

Figure 1: (a) A DBR-metal microcavity with a J-aggregate excitonic layer and a total optical thickness of ~λ/2 where λ = 595 nm. (b) The reflectivity of devices having different cavity-exciton detunings and the corresponding PL.

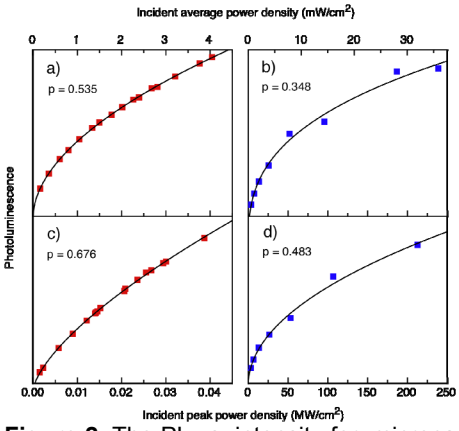

Figure 2: The PL vs. intensity for: microcavity pumped with 535 nm (a) 10 ns laser (b) 150 fs laser; and a J-aggregate thin film pumped same two lasers.

References

D. G. Lidzey, D. D. C. Bradley, M. S. Skolnick, T. Virgili, S. Walker, and D. M. Whittaker, "Strong exciton-photon coupling in an organic semiconductor microcavity," Nature, vol. 395 pp. 53-55, 1998.

J. R. Tischler, M. S. Bradley, Q. Zhang, T. Atay, A. Nurmikko, and V. Bulović, "Solid state cavity QED: Strong coupling in organic thin films," Organic Electronics vol. 8, no. 2-3, pp. 94-113, 2007.

M. S. Bradley, J. R. Tischler, and V. Bulović, "Layer-by-layer J-aggregate thin films with a peak absorption constant of 10(6) cm(-1)," Advanced Materials, vol. 17, no. 15, pp. 1881-1884, 2005.

L. Kelbauskas, S. Bagdonas, W. Dietel, and R. Rotomskis, "Excitation relaxation and structure of TPPS4 J-aggregates," Journal of Luminescence, vol. 101, pp. 253-262, 2003.

10. Strong Light-matter Coupling Using a Robust Non-cyanine Dye J-aggregate Material

Sponsors
Institute for Soldier Nanotechnology

Project Staff
J. R. Tischler, G. M. Akselrod, M. S. Bradley, J. Chan, E. R. Young, D. G. Nocera, T. M. Swager, V. Bulović

We demonstrate strong light-matter coupling using a promising new J-aggregate material based on a dibenz[a,j]anthracene macrocycle [1], Figure 1a, that is robust under high power optical excitation. Strong light-matter coupling leads to polaritonic resonances that are superpositions of the underlying excitonic and photonic states [2] and can exhibit laser-like coherent light emission at remarkably low excitation densities due to polariton condensation [3]. A key hindrance to achieving polariton condensation thus far using cyanine dye J-aggregates has been exciton-exciton annihilation [4], which quenches excitations from the polaritonic states before they can condense. The J-aggregates of the dibenz[a,j]anthracene-based macrocycle show no signs of exciton-exciton annihilation until optical excitation densities exceeding 20 MW/cm^2, while in thin films of a typical J-aggregated cyanine dye, TDBC, annihilation appears at 10 kW/cm^2. Thin films of the macrocycle were prepared by spin-coating a 6 mg/ml solution of the dye in chlorobenzene, yielding layers that were 15 nm thick with an RMS roughness of less than 1 nm. The J-aggregation of the dye in these films was evidenced by the appearance of a narrow absorption line at 465 nm of FWHM = 15 nm, Figure 1b, and the concomitant disappearance of the monomer absorption band as the dye concentration was increased [1]. The films possess an absorption coefficient of 2.1 x 10^5 cm^{-1} at the J-aggregate absorption peak wavelength of 465 nm, show good photochemical stability, and have photoluminescence quantum yield exceeding 90%. Strong coupling was observed when thin films of the macrocycle were situated in a λ/2n planar optical microcavity consisting of a silver mirror and dielectric Bragg reflector. Devices exhibit polaritonic dispersion with a room temperature Rabi-splitting of 130 meV, Figure 2. Experiments are underway to demonstrate organic-based polariton condensation.

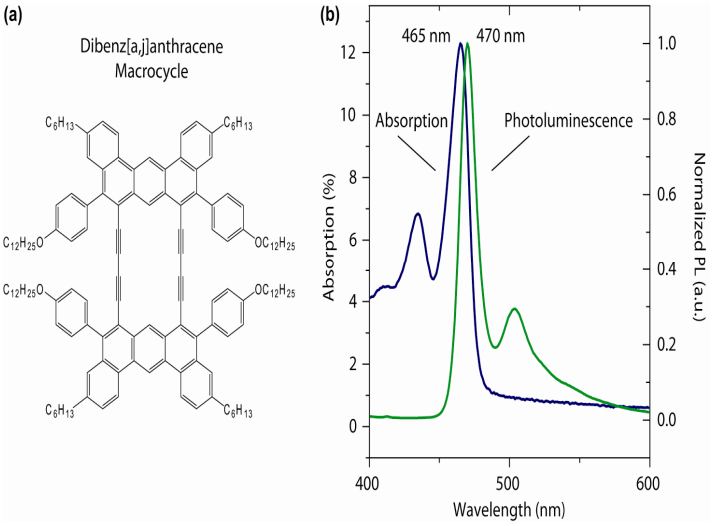

Figure 1: (a) Chemical structure of dibenz[a,j]anthracene-based macrocycle. (b) Optical absorption and photoluminescence spectra from a thin film prepared by spin-coating the compound onto a glass substrate. Thin film roughness of less than 1 nm was observed in AFM.

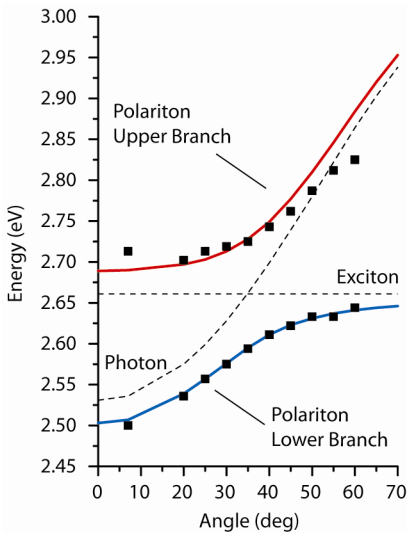

Figure 2: Polaritonic dispersion relation derived from angular device reflectance data. Anti-crossing of energy levels is observed at 35º from normal.

References

J. M. W. Chan, J. R. Tischler, S. E. Kooi, V. Bulović, T. M. Swager, "Synthesis of J-Aggregating dibenz[a,J]anthracene-based macrocycles", Journal of the American Chemical Society, vol. 131, pp. 5659-5666, April 2009.

C. Weisbuch, M. Nishioka, A. Ishikawa, and Y. Arakawa, "Observation of the coupled exciton-photon mode splitting in a semiconductor quantum microcavity", Physical Review Letters, vol. 69, pp. 3314 – 3317, May 1992.

J. Kasprzak J, M. Richard, S. Kundermann, A. Baas, P. Jeambrun, J. M. J. Keeling, F. M. Marchetti, M. H. Szymanska, R. Andre, J. K. Staehli, V. Savona, P. B. Littlewood, B. Deveaud, L. S. Dang, "Bose-Einstein condensation of exciton polaritons", Nature, vol. 443, pp. 409-414, September 2006.

J. Moll, W. J. Harrison, D. V. Brumbaugh, A. A. Muenter, "Exciton annihilation in J-aggregates probed by femtosecond fluorescence upconversion", Journal of Physical Chemistry A, vol. 104, pp. 8847-8854, October 2000.

11. Molecules as Segmented Storage Elements in Floating Gate Memories

Sponsors
SRC/FCRP Focus Center on Materials Structures and Devices

Project Staff
S. Paydavosi, V. Bulović

Conventional flash memories may reach fundamental scaling limits [1] because of the minimum tunnel oxide thickness and poor charge retention due to defects in the tunneling oxide, necessitating new approaches to meet the scaling requirements while simultaneously meeting the reliability and performance requirements of future products. In this study we demonstrate alternative nano-segmented floating gate memories using organic molecules as programmable charge-storage and charge-retention elements in capacitive structures. These organic thin films consist of inherently well-ordered planner molecules that are on the order of 1nm in size, representing a uniform set of identical nanostructured charge-storage centers. We investigated and compared the memory behavior of a variety of molecular thin films for identifying the molecular thin-film characteristics best suited for design of floating gate memory. The initial results show device durability over 10^5 program-erase cycles, with a hysteresis window of up to 3.3 V for program/erase conditions of +8V/-8V, corresponding to the charge storage density of 5 x 10^{12} cm^{-2}. These results signify the potential of using molecular organic thin films as a floating gate of flash memory devices.

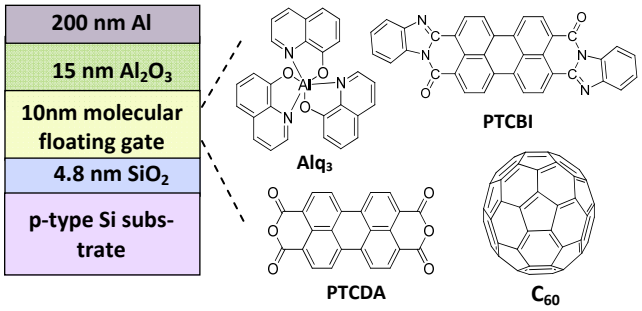

Figure 1: The schematic cross-section of the device structure with chemical structures of tested molecular organic thin films.

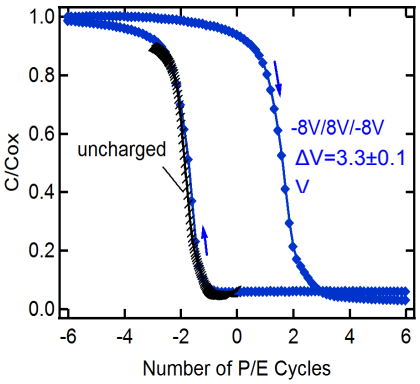

Figure 2: The *C-V* plot of a device with a10-nm thick PTCBI layer showing a 3.3±0.1 V hysteresis window.

References

Pavan, P., Bez, R., Olivo, P. & Zanoni, E. Flash Memory Cells-An Overview. Proceedings of the IEEE 85, 8 (1997).

12. Direct Patterning of Metallic MEMS through Microcontact Printing

Sponsors
DARPA, Hewlett-Packard

Project Staff
C. E. Packard, A. Murarka, V. Bulović

Standard photolithography-based methods for fabricating microelectromechanical systems (MEMS) present several drawbacks including expense, incompatibility with flexible substrates, and limitations to wafer-sized device arrays. We have developed a new fabrication method for rapid fabrication of large-area MEMS that breaks the paradigm of lithographic processing using a scalable, large area microcontact printing method to define three-dimensional electromechanical structures. Our PDMS Lift-Off Transfer (PLOT) involves the rapid removal of a pick-up stamp from a transfer pad to transfer a continuous metal film from the pad to the stamp. A stamp that forms the membrane suspension supports is fabricated by molding a thin layer of PDMS against a silicon master with a predefined relief. The metal membranes are deposited by thermal evaporation onto a transfer pad which has been prepared with an organic molecular release layer. To achieve transfer of the metal membrane over the supports of the device, the stamp is brought into conformal contact with the transfer pad and then released by rapidly peeling away. MEMS bridge structures, such as the ones shown in Figure 1, have been fabricated using PLOT, and their performance as variable capacitors has been characterized. In Figure 2, the capacitance of these devices increases with applied voltage, indicating mechanical deflection of the bridges due to the electrostatic force. PLOT forms MEMS structures without requiring elevated temperature processing, high pressure, or wet chemical or aggressive plasma release etches, providing compatibility with sensitive material sets for the fabrication of integrated micro- or opto-electronic/MEMS circuits. Flexible, paper-thin device arrays produced by this method may enable such applications as pressure sensing skins for aerodynamics, phased array detectors for acoustic imaging, and novel adaptive-texture display applications.

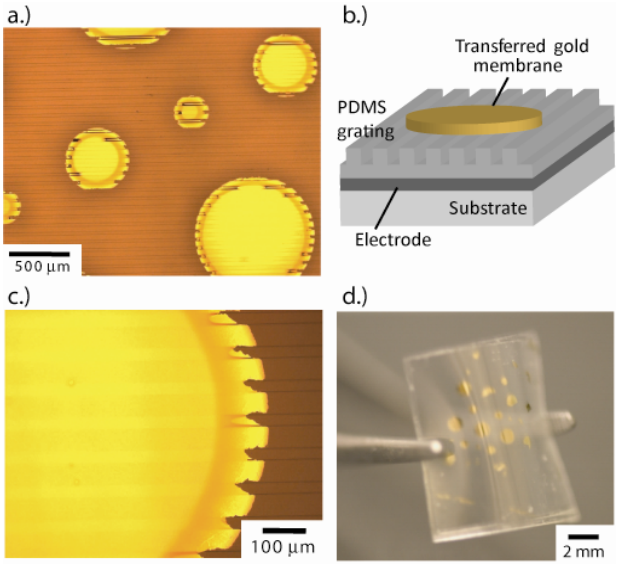

Figure 1: Devices formed by PLOT: optical micrographs (a. & c.), schematic (b.) and photograph of devices formed on a flexible substrate (d.)

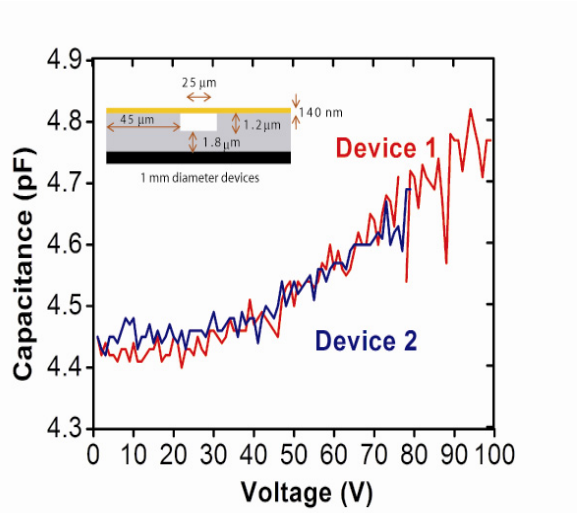

Figure 2: Capacitance increases with applied voltage in two devices, indicating mechanical deflection of the bridging metal film.

13. Surface Micromachining via Digital Patterning

Sponsors
DARPA, Hewlett-Packard

Project Staff
E.W. Lam, H. Li, V. Bulović, M.A. Schmidt

Conventional microelectromechanical systems (MEMS) fabrication relies heavily on the semiconductor manufacturing paradigm. While this model is well-suited for planar devices such as integrated circuits, it is drastically limited in the design and fabrication of three-dimensional devices such as MEMS. From a commercial viewpoint, this paradigm also poorly fits MEMS because the lower market demand makes it harder to offset the high production costs. Ridding MEMS fabrication of its reliance on such techniques may introduce several advantages, namely a wider base of substrate materials as well as decreased manufacturing costs.

Our project investigates severing MEMS fabrication from the traditional paradigm via digital patterning technologies. We have previously shown how MEMS can be used for the direct patterning of small molecular organics [1]. Using similar concepts, we have shown that surface micromachining can also be achieved.

In 2007-2008, we identified a viable material set for our surface micromachining process' sacrificial and structural layers: poly-methylmethacrylate (PMMA) and silver nanoparticles. To account for surface non-uniformity of the deposited PMMA, we employed solvent vapors to effectively lower the polymer's glass transition temperature and cause reflow at room temperatures [2]. To limit surface wetting and increase material loading of the silver nanoparticles, we deposited a PMMA reservoir to contain the silver nanoparticle solution (Figure 1). Free-standing cantilevers were fabricated (Figure 2), confirming that these techniques can be used for a surface micromachining process.

The next stage will be to fabricate additional MEMS structures and test the silver nanoparticle's mechanical properties. These properties will be used to design and fabricate a demonstration system based on our surface micromachining process. Subsequent stages will include creating a library of digital fabrication processes so that entire MEMS devices can be fabricated without the use of semiconductor manufacturing techniques.

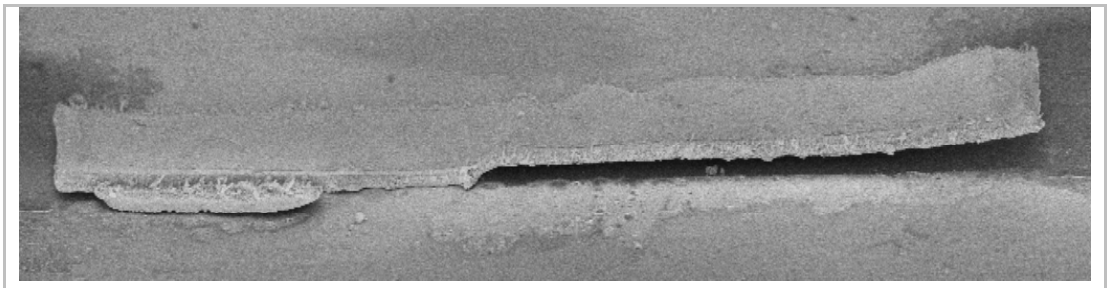

Figure 1: A silver surface micromachined cantilever fabricated using direct printing.

References

J. Chen, V. Leblanc, S.-H. Kang, M.A. Baldo, P.J. Benning, V. Bulović, and M.A. Schmidt, "Direct patterning of organics and metals using a micromachined printhead," in Proc. MRS Spring 2005, San Francisco, CA, Mar./Apr. 2005, pp. H1.8:1-7

J. Feng, M. Winnik, R.R. Shivers, and B. Clubb, "Polymer blend latex films: morphology and transparency," Macromolecules, vol. 28, no. 23, pp. 7671-7682, Nov. 1995.

14. Effects of Bias Stress in Organic Thin-film Transistors

Sponsors
FCRP Focus Center for Circuit and Systems Solutions (C2S2)

Project Staff
K. Ryu, I. Nausieda, D. He, A. I. Akinwande, V. Bulović, C. G. Sodini

Organic transistor technology holds the promise of large-area flexible electronics and integration of various sensors and actuators on a single substrate [1]. However, current-voltage (I-V) characteristics of organic transistors are known to change with the application of prolonged voltages [2]. Such change, termed the bias-stress effect, leads to operational instability, which limits the usable lifetime of the circuit. The bias-stress effect must be understood and minimized to enable the use of organic transistors in functional applications. In this work, we present a method to accurately measure the bias-stress effect and a model that predicts the effect at different stress conditions. The model provides physical insight into the mechanisms causing the bias-stress effect and an estimate of the expected lifetime of the transistor. It also provides a means to determine the operating region that minimizes the bias-stress effect.

To measure the bias-stress effect and no other degradation effects, we characterize pentacene OTFTs that have no measurable change due to storage in nitrogen ambient. We demonstrate that the after-stress I-V characteristics can be accurately described by the initial I-V characteristics and a shift in applied gate voltage, ΔV. Based on this observation, we characterize the bias-stress effect with ΔV. We measure ΔV at different gate and drain bias (V_{SG} and V_{SD}) and stress times. Measurements with different V_{SD} at fixed V_{SG} stress show that ΔV decreases with increasing drain bias or current, indicating that gate field and channel carriers, not drain current, are responsible for the stress effect. We report that ΔV saturates independent of the V_{SG} stress. We propose a simple carrier-trapping rate model that results in a stretched-exponential equation that accurately describes the observed ΔV behavior with respect to stress times. The model suggests that the bias-stress effect is caused by trapping of the channel carriers. The bias-stress effect saturates due to a constant number of trap sites, unlike in a-Si:H TFTs, where the trap sites are continually created until there are no more channel carriers [3]. The saturation of the bias-stress effect independent of the V_{SG} stress is reported for the first time in organic transistors.

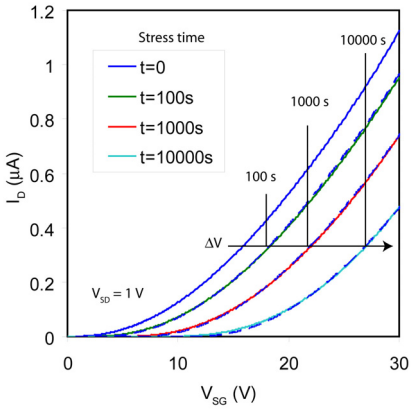

Figure 1. Transfer characteristics after bias stress at V_{SG} = 30 V, V_{SD} = 1 V at varying stress time, t. The dashed line shows the shifted transfer characteristics of the unstressed device (t = 0 s).

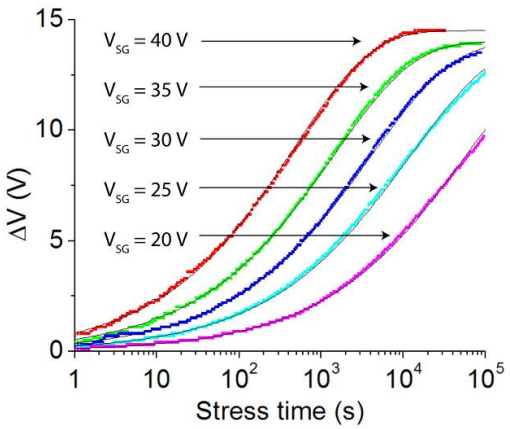

Figure 2. Measured stress time-dependence of the induced ΔV for different gate bias-stress conditions (colored dots) and the stretched-exponential fit made to the data (solid lines).

References:
I. Nausieda, K. Ryu, I. Kymissis, A.I. Akinwande, V. Bulović, C.G. Sodini, "An organic active-matrix imager," IEEE Transactions on Electron Devices, vol.55, pp. 527-532, Feb. 2008.
S. J. Zilker, C. Detcheverry, E. Cantatore, and D. M. de Leeuw, "Bias stress in organic thin-film transistors and logic gates," Appl. Phys. Lett. 79, 1124, Aug. 2001.
W. B. Jackson, J. M. Marshall, M. D. Moyer, "Role of hydrogen in the formation of metastable defects in hydrogenated amorphous silicon," Phys. Rev. B, 39, pp. 1164 – 1179, 1989.

15. An Organic Thin-film Transistor Circuit for Large-area Temperature-sensing

Sponsors
FCRP Focus Center for Circuit and Systems Solutions (C2S2), Hewlett Packard, NSERC Fellowship

Project Staff
D. He, I. Nausieda, K. Ryu, A. I. Akinwande, V. Bulović, C. G. Sodini

The organic thin-film transistor (OTFT) is a field-effect transistor technology that uses organic materials as the semiconductor. OTFTs have field-effect mobilities that are comparable to those of hydrogenated amorphous silicon TFTs, and OTFTs are compatible with large-area and mechanically-flexible substrates [1], [2]. The goal of this work is to demonstrate an integrated OTFT temperature-sensing circuit suitable for large-area and flexible substrates.

As shown in Figure 1, two important differences are observed between the OTFT's and the MOSFET's current-voltage characteristics when temperature is varied. First, the OTFT's current increases with temperature in both subthreshold and above-threshold regimes, whereas the MOSFET's above-threshold current decreases with temperature. Second, the OTFT's subthreshold slope is temperature independent over the measured range of -20 to 60°C, while the MOSFET's subthreshold slope is proportional-to-absolute-temperature (PTAT).

Because of these differences in temperature response, the OTFT temperature-sensing "ΔV_{BE} circuit" (Figure 2a) has a complementary-to-absolute-temperature (CTAT) response instead of an equivalent silicon circuit's PTAT response. The OTFT circuit is scaled to an array format to enable surface thermal sensing applications. As Figure 2b shows, the array consists of 3x3 temperature-sensing circuit cells of $1mm^2$ each and is currently being characterized.

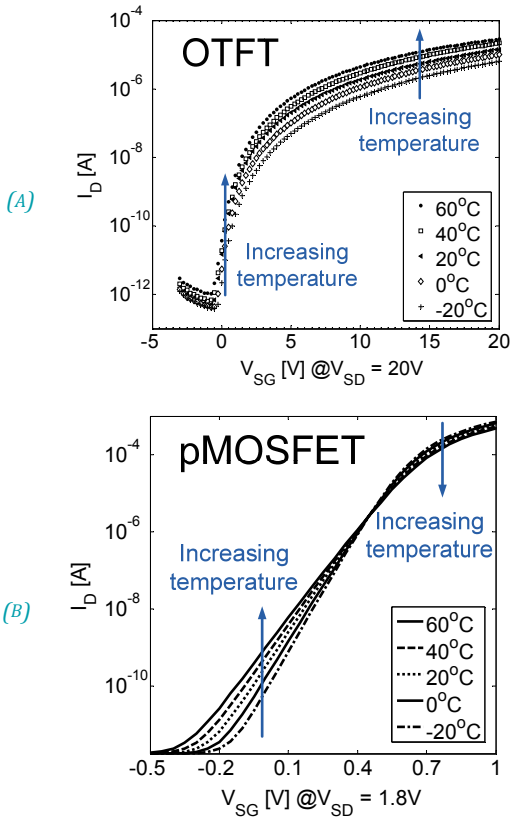

Figure 1: (a) The OTFT's (measured) and (b) pMOSFET's (BSIM3) current-voltage characteristics versus temperature.

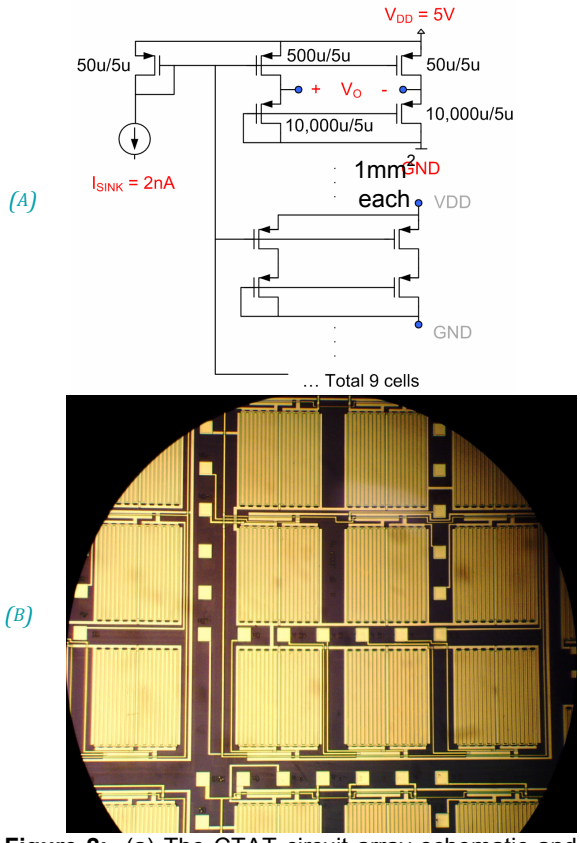

Figure 2: (a) The CTAT circuit array schematic and (b) die photo.

References:

Y.Y. Lin, D.J. Gundlach, and T.N. Jackson, "High-mobility pentacene organic thin film transistors," Device Research Conference Digest, June 1996, pp. 80–81.

I. Kymissis, C.G. Sodini, A.I. Akinwande, and V. Bulović, "An organic semiconductor based process for photodetecting applications," IEEE International Electron Devices Meeting Technical Digest, Dec. 2004, pp. 377–380.

16. Dual-threshold-voltage Organic Thin-film Transistors for Mixed-signal Integrated Circuits

Sponsors
FCRP Focus Center for Circuit and Systems Solutions (C2S2), Martin Family Fellowship

Project Staff
I. Nausieda, K. Ryu, D. He, A. I. Akinwande,V. Bulović, C. G. Sodini

Organic thin-film transistors (OTFTs) hold the potential for large-area, flexible electronics because their near-room-temperature processing enables them to be fabricated on plastic substrates. We have developed a low temperature (≤95°C) process to fabricate integrated OTFTs [1]. Designing circuits using OTFTs is challenging since only p-channel transistors are typically available. The OTFT technology limits noise margins in digital circuits due to the lack of an NMOS load, the location of the threshold voltage (V_T), and the availability of a single V_T device [2]. We have addressed this problem by creating a dual V_T process, with the addition of only one mask to pattern a second gate metal. We present positive noise margin inverters and a near rail-to-rail ring oscillator using a 3V supply. The ring oscillator output waveform is shown in Figure 1.

The dual V_T process enables analog integrated circuits. We demonstrate an uncompensated, two-stage operational amplifier with open loop gain of 36dB, unity gain frequency of ~7Hz, and common-mode rejection ratio (CMRR) of 20.1dB. The dual V_T op amp has 30x better gain * -3dB frequency product than a single V_T implementation and uses a 5V power supply. The op-amp frequency response is pictured in Figure 2.

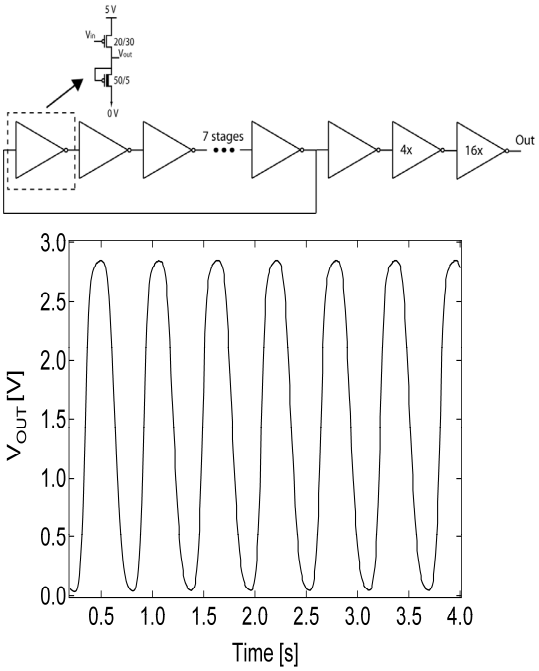

Figure 1: Schematic of 11-stage ring oscillator and buffer (top). A 1.7 Hz output transient, indicating an inverter propagation delay of 27 ms.

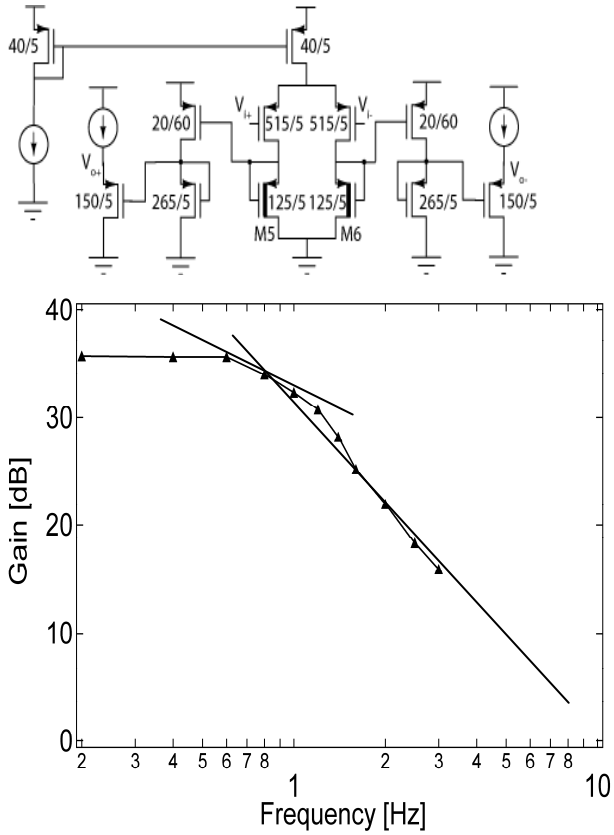

Figure 2: Schematic of op-amp (top). Open loop frequency response of dual V_T operational amplifier, indicating 2 poles (bottom).

References:

I. Nausieda, K. Ryu, I. Kymissis, A.I. Akinwande, V. Bulović, C.G. Sodini, "An organic active-matrix imager," IEEE Transactions on Electron Devices, vol.55, pp. 527-532, Feb. 2008.

E. Cantatore, T.C.T. Geuns, G. Gelnick, E. van Veenendaal, A.F.A. Gruijthuijsen, L. Schrijnemakers, S. Drews, D.M de Leeuw, "A 13.56-MHz RFID system based on organic transponders," IEEE Journal of Solid-State Circuits, vol.42, pp.84-92. Jan. 2007.

17. Reproducible Lithographically Patterned Metal-oxide Transistors for Large-area Electronics

Sponsors
DARPA / FCRP Focus Center for Circuit and Systems Solutions (C2S2)

Project Staff
A. Wang, B. Yaglioglu, C. G. Sodini, V. Bulović, A. I. Akinwande

Metal-oxide-based field-effect transistors (FETs) have been demonstrated with higher charge-carrier mobilities, higher current densities, and faster response performance than amorphous silicon FETs, which are the dominant technology used in display backplanes [1], [2]. Because the optically transparent semiconducting oxide films can be deposited at near-room temperatures, these materials are compatible with future generations of large-area electronics technologies that require flexible substrates [3]. Our project aims to develop a low-temperature, scalable lithographic process for metal oxide-based FETs that can be integrated into large-area electronic circuits.

While any single demonstrated transistor may have excellent characteristics, circuit design using these FETs is impossible without the capability to reproducibly fabricate FETs with uniform characteristics. Previously, we demonstrated top-gate, fully lithographic FETs of varying channel lengths on 100-mm glass wafers with a sputtered $ZnO:In_2O_3$ channel layer, using an organic polymer, parylene, as the gate dielectric and indium-tin-oxide (ITO) for source/drain contacts. Because of process non-uniformities, however, FET turn-off voltages (V_{OFF}) across a wafer and between wafer lots varied by as much as ±10V. By modifying the process to deposit semiconductor and protective dielectric together without breaking vacuum, the FET uniformity across wafers was improved; the standard deviation of V_{OFF} decreased to <1V across three subsequently-processed wafer lots. Figure 1 shows a photograph of a 100-mm glass after fabrication was completed; current-voltage characteristics for a device fabricated in the improved process are shown in Figure 2. This baseline process can provide a platform for the design of oxide FET-based circuits, as well as for studying the underlying device physics of metal-oxide FETs.

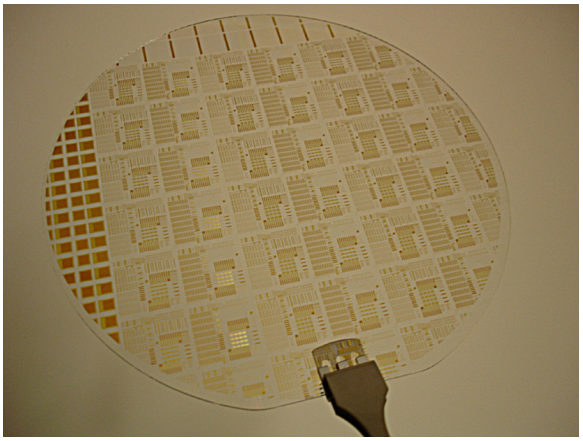

Figure 1: A 100-mm glass wafer with lithographically patterned metal-oxide field-effect transistors. Device uniformity can be examined by comparing transistors of the same geometry from different die across the wafer.

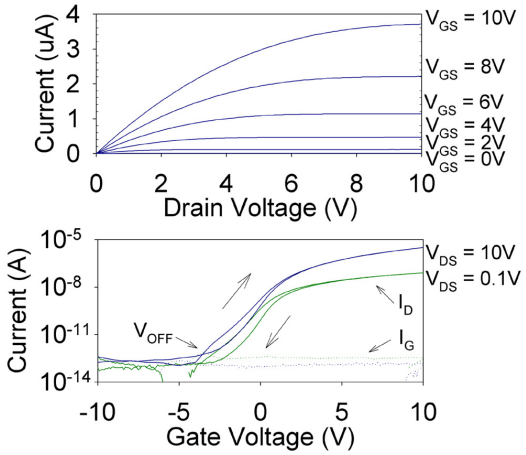

Figure 2: Current-voltage characteristics of lithographically patterned FET (W/L = 100μm / 100μm). Output curves are plotted in the top graph; double-swept transfer curves taken in saturation and triode regions are plotted on the bottom. The turn-off voltage, V_{OFF}, is -4V.

References:

R.L. Hoffman, B.J. Norris, and J.F. Wager, "ZnO-based transparent thin-film transistors," Applied Physics Letters, vol. 82, no. 5, pp. 733-735, Feb. 2003.

K. Nomura, H. Ohta, A. Takagi, T. Kamiya, M. Hirano, and H. Hosono, "Room-temperature fabrication of transparent flexible thin-film transistors using amorphous oxide semiconductors," Nature, vol. 432, pp. 488-492, Nov. 2004.

E. Fortunato, P. Barquinha, A. Pimentel, A. Goncalves, A. Marques, L. Pereira, and R. Martins, "Fully transparent ZnO thin-film transistor produced at room temperature," Advanced Materials, vol. 17, pp. 590-594, Mar. 2005.

18. Stability of Metal Oxide-based Field-effect Transistors

Sponsors
Hewlett-Packard, DARPA

Project Staff
B. Yaglioglu, A. Wang, K. Ryu, C. Sodini, A. I. Akinwande, V. Bulović

The main goal of this research is to combine a low-temperature budget fabrication method with scalable processes such as sputter deposition to realize oxide channel field-effect transistors (FETs) on glass or flexible plastic substrates. Oxide-based transistors offer an attractive alternative to commercially used amorphous Si transistors due to their high mobility values (~10-20cm^2/Vs vs ~1cm^2/Vs) [1-3]. Field-effect mobility, sub-threshold slope, and threshold voltage of FETs are the main parameters that are characterized for circuits. However, reliability of properties needs to be also addressed before these devices take their place in large-area electronic applications.

In this study we test the stability of FETs that have a polymer dielectric, parylene, and an amorphous oxide semiconductor, zinc indium oxide. The devices are processed lithographically at low temperatures (T ≤ 100 ºC). Figure 1 shows a typical transfer characteristics curve representing device performance. The inset gives the distribution of the threshold voltage across a 4-inch wafer. In Figure 2, the change in I-V characteristics is shown under a prolonged gate bias stress. The gate bias is interrupted at fixed times to record the transfer characteristics of the transistor at a drain bias of V_D=1V. Preliminary results of I-V tests show a positive shift in the threshold voltage. Two possible mechanisms that are originally proposed for similar shifts in amorphous Si FET's are metastable state generation in the semiconductor and charge trapping in the dielectric [4]. Stability experiments at different temperatures and bias gate voltages are conducted to understand the instability mechanisms in these hybrid (inorganic/organic) devices.

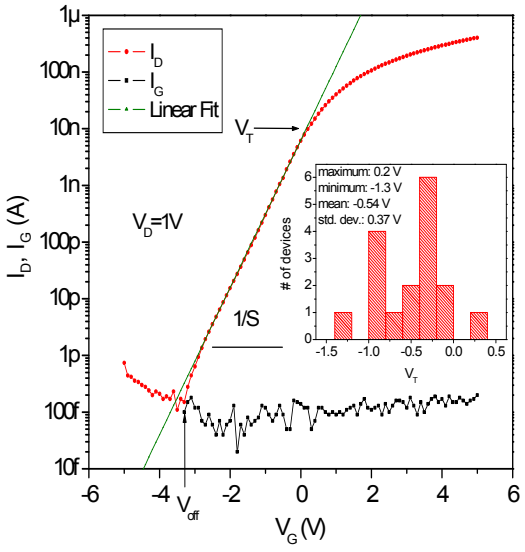

Figure 1: Transfer characteristics of a W/L=100µ/100µ transistor. Data are taken from -5V to 5V with 0.1V steps while V_D= 1V. The distribution of threshold voltage collected from 17 devices on different dies across the wafer is given in the inset.

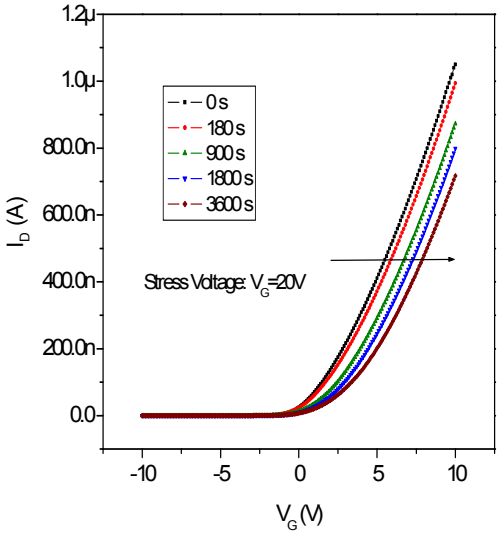

Figure 2: The V_G-I_D curve of a transistor as a function of stress time. The stress measurement is interrupted every 180s to measure the transfer characteristics. Measurements after 3min, 15min, 30min, and 1h are included to show the shift in the characteristics.

References

P.F. Carcia, R.S McLean, M.H. Reilly, and G. Nunes, "Transparent ZnO thin film transistors fabricated by rf magnetron sputtering," Applied Physics Letters, vol. 82, no. 7, pp. 1117-1119, Feb. 2003

N.L. Dehuff, E.S. Kettenring, D. Hong, H.Q. Chiang, J.F. Wager, R.L. Hoffman, C.H. Park, and D.A. Keszler, “Transparent thin film transistors with zinc indium oxide channel layer,” Journal of Applied Physics, vol. 97, no. 6, pp. 064505:1-5, Mar. 2005.

H. Kumomi, K. Nomura, T. Kamiya, and H. Hosono, “Amorphous oxide channel TFTs,” Thin Solid Films, vol. 516, no. 7, pp.1516-1522, Feb. 2008.

M.J. Powell, C. van Berkel, and J R. Hughes, “Time and temperature dependence of instability mechanisms in amorphous silicon thin-film transistors,” Applied Physics Letters, vol. 54, no.14, pp. 1323-1325, Jan. 1989.

Publications

Journal Articles, Published

C. Madigan, E. Howe, V. Bulović, P. Mardilović, P. Kornilovitch, “Planarization in electrochemically fabricated nanodimensional films,” *Journal of Physical Chemistry C* 112, 7318 (2008).

I. Nausieda, K. Ryu, I. Kymissis, A. Akinwande, V. Bulović, C.G. Sodini, “An Organic Active-Matrix Imager,” *IEEE Transactions on Electron Devices* 55, 527 (2008).

J.M. Caruge, J.E. Halpert, V. Wood, V. Bulović, and M.G. Bawendi, “Colloidal Quantum-Dot Light-Emitting Diodes with Metal-Oxide Charge Transport Layers,” *Nature Photonics* 2, 247 (2008).

J. Yu and V. Bulović, “Using Integrated Optical Feedback to Counter Pixel Aging and Stabilize Light Output of Organic LED Display Technology,” *IEEE Journal of Display Technology* 4, 308 (2008).

J. Ho, A. Arango, and V. Bulović, “Lateral Organic Bi-layer Heterojunction Photoconductors,” *Applied Physics Letters* 93, 063305 (2008).

P.O. Anikeeva, C.F. Madigan, J.E. Halpert, M.G. Bawendi, V. Bulović, “Electronic and Excitonic Processes in Light-Emitting Devices Based on Organic Materials Colloidal Quantum Dots,” *Physical Review B* 78, 085434, (2008).

M.S. Bradley, J.R. Tischler, Y. Shirasaki, and V. Bulović, “Predicting the Linear Optical Response of J-aggregate Microcavity Exciton-Polariton Devices,” *Physical Review B* 78, 193305 (2008).

L. Kim, P.O. Anikeeva, S.A. Coe-Sullivan, J.S. Steckel, M.G. Bawendi, and V. Bulović, "Contact Printing of Quantum Dot Light-Emitting Devices," *Nano Letters* 8, 4513 (2008).

A.C. Arango, D.C. Oertel, Y. Xu, M.G. Bawendi, and V. Bulović, "Heterojunction Photovoltaics Using Printed Colloidal Quantum Dots as a Photosensitive Layer," *Nano Letters* 9, 860 (2009).

T.P. Osedach, S.M. Geyer, J.C. Ho, A.C. Arango, M.G. Bawendi, and V. Bulović, "Lateral Heterojunction Photodetector Consisting of Molecular Organic and Colloidal Quantum Dot Thin Films," *Applied Physics Letters* 94, 043307 (2009).

A. Reina, X. Jia, J. Ho, D. Nezich, H. Son, V. Bulović, M.S. Dresselhaus, and J. Kong, "Large Area, Few-Layer Graphene Films on Arbitrary Substrates by Chemical Vapor Deposition," *Nano Letters* 9, 30 (2009).

J.E. Halpert, J.R. Tischler, G. Nair, B.J. Walker, W. Liu, V. Bulović, M.G. Bawendi, “Electrostatic Formation of Quantum Dot/J-aggregate FRET Pairs in Solution,” *Journal of Physical Chemistry C* 113, 9986 (2009).

V. Wood, M.J. Panzer, J. Chen, M.S. Bradley, J.E. Halpert, M.G. Bawendi, and V. Bulović, "Inkjet-Printed Quantum Dot–Polymer Composites for Full-Color AC-Driven Displays," *Advanced Materials* 21, 2151 (2009).

V. Wood, J.E. Halpert, M.J. Panzer, M.G. Bawendi, V. Bulović, "Alternating Current Driven Electroluminescence from ZnSe/ZnS:Mn/ZnS Nanocrystals," *Nano Letters* 9, 2367 (2009).

J. Mei, M.S. Bradley, V. Bulović, "Photoluminescence quenching of tris-(8-hydroxyquinoline) aluminum thin films at interfaces with metal oxide films of different conductivities," *Physical Review B* 79, 235205 (2009).

J.M.W. Chan, J.R. Tischler, S.E. Kooi, V. Bulović, T.M. Swager "Synthesis of J-Aggregating Dibenz[a,J]anthracene-Based Macrocycles," *Journal of American Chemical Society* 131, 5659 (2009).

Theses

Ph.D. Thesis:

Yu, J. (V. Bulović), "Improving OLED Technology for Displays," Sep. 2008 (EECS).

Anikeeva, P. (V. Bulović), "Physical Properties and Design of Light-Emitting Devices Based on Organic Materials and Nanoparticles," Feb. 2009 (DMSE).

Bradley, M.S. (V. Bulović), "Engineering J-Aggregate Cavity Exciton-Polariton Devices," June 2009 (EECS).

Ho, J. (V. Bulović), "Organic Lateral Heterojunction Devices for Vapor-phase Chemical Detection," June 2009 (EECS).

M.Eng. Thesis:

Shirasaki, Y. (V. Bulović), "Efficient Förster Energy Transfer From Phosphorescent Organic Molecules to J-aggregate Thin Film," February 2008 (EECS).

Abdu, H. (V. Bulović), "Molecular and Quantum Dot Floating Gate Non-Volatile Memories," June 2008 (EECS).

Friend, D. (V. Bulović), "Theory and Fabrication of Evanescently-Coupled Photoluminescent Devices," June 2008 (EECS).

Tang, H. (V. Bulović), "Near Room Temperature Lithographically Processed Metal-Oxide Transistors," June 2008 (EECS).